IDENTIFICATION OF THE BASELINE MODAL PARAMETERS OF THE CARQUINEZ SUSPENSION BRIDGE USING AMBIENT VIBRATION DATA

Raimondo Betti and Ah Lum Hong

Department of Civil Engineering and Engineering Mechanics
Columbia University, New York

Abstract

The identification of modal parameters has been performed for the New Carquinez suspension bridge in California. By using multiple ambient vibration data sets recorded through a wind-motion monitoring system in the bridge, the baseline modal parameters were obtained in order to investigate dynamic behavior of the bridge in operating conditions. For the modal parameters identification, the data-driven stochastic subspace identification technique was implemented. For each data set, the modal parameters for structural modes were estimated by examining the estimation error between measured data and reconstructed one from the identified modes. Based on the results, variability of the identified modal parameters was also investigated.

Introduction

The Newly built Carquinez suspension bridge (NCB) linking Vallejo with Crockett in California is located in a windy area and near three active earthquake faults (the San Andreas Fault, the Hayward Fault, and the Franklin Fault). For structural health monitoring of this bridge in operational condition, the Strong Motion Instrumentation Program (SMIP) has devised a wind-motion monitoring system as well as an earthquake monitoring system by installing accelerometers over the bridge. Since, in vibration based structural health monitoring, the evaluation of a structure's global dynamical behavior requires past or undamaged state information of the structure as a baseline, having precise baseline dynamic properties of the structure is important in order to assess such a structure's condition in the future.

When only structural responses are available for the characterization of a structure's dynamic properties, as it is in ambient vibration cases, stochastic system identification techniques are usually implemented to identify its modal parameters (natural frequencies, damping ratios, and mode shapes). Peeters and De Roeck [1] reviewed currently used stochastic system identification techniques in both frequency and time domains. Among such techniques, Frequency Domain Decomposition (FDD) technique in frequency domain and Stochastic Subspace Identification (SSI) technique in time domain are showing great promise, especially in detecting closely spaced modes [2]. However, despite of attempts to further improve efficiency of such techniques [3][4], they are still in need of improvement since results from both the techniques are quite sensitive to choices of certain parameters in their implementations. In comparing the FDD and SSI techniques, Brincker *et al*. [5] showed that the FDD technique has less uncertainty on damping estimates than the data driven SSI technique; however, the results from the FDD were significantly affected by the frequency resolution and so, consequently, by

the length of time histories. In fact, the authors concluded that at least 1 hour long time histories were required for a proper estimation of damping ratios.

In this study, the data driven SSI technique was implemented for modal parameters identification in order to build baseline modal parameters of the NCB using 17 ambient vibration data sets recorded from the bridge in operating condition. To this end, practical issues in the implementation of data-driven SSI technique were first investigated and an efficient way of identifying modal parameters from this technique was proposed. After that, certain bounds of modal parameter estimates for each identified mode were provided.

Ambient Vibration Data

Sensor Configuration

As a part of the SMIP monitoring of the NCB, 76 accelerometers were placed on towers, piers, abutments, anchorages, piles of the towers as well as on the bridge deck for monitoring earthquake induced motions of this bridge. Among such 76 accelerometers, a set of ten accelerometers on the northern half of the deck also belongs to the wind-motion monitoring system, with a supplement of an anemometer placed at the mid-span. Figure 1 displays the locations of such ten accelerometers (six in vertical, three in transverse, and one in longitudinal directions) in the wind-motion monitoring system. The purpose of this wind-motion monitoring system is to record the dynamic behavior of this bridge under ambient excitations (i.e. wind and traffic loadings).

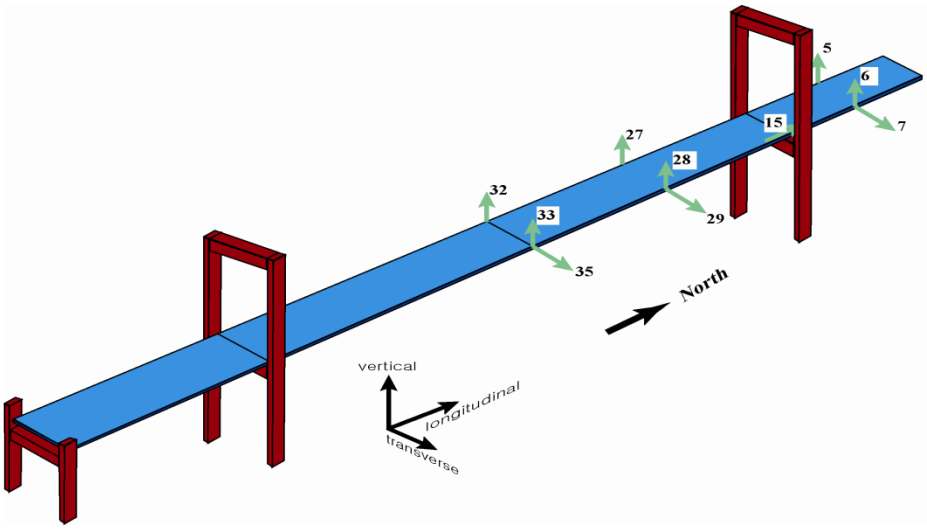

Figure 1. Locations of the sensors belonging to the wind-motion monitoring system

Measurement Properties

A total of 21 data sets of ambient vibration responses were recorded through either the wind-motion or earthquake monitoring systems. Table 1 indicates the recording date, start time,

and duration of each data set as well as wind information in terms of the mean wind direction (D_v) and the mean of wind speed (V_v) along the mean wind direction. Data sets #1 to 4 were measured on windy days and data sets #5 to 8 at the same time (10:00pm) for four days in February. Furthermore, in order to examine a change in modal parameters during the day and night time, data sets #9 to 21 were recorded at different times from afternoon to midnight for three days in May. The data sets also have various record lengths from 54 sec (data set #3) to 1068 sec (data set #10).

Among the 21 data sets, structural responses of data sets #3 and 8 were measured through the earthquake monitoring system with the sampling frequency of 200 Hz while the other sets through the wind-motion monitoring system with 20 Hz of the sampling frequency. Since the anemometer does not belong to the earthquake monitoring system, wind information was not provided for data sets #3 and 8.

In this study, only 17 data sets that have the record lengths of at least 10 minutes were considered for the identification of the NCB's modal parameters.

Table 1. Ambient vibration data information

Data Set #	Date	Time	Length	Wind	
				V_v [m/s]	D_v[^{o}]
1	27-Feb-06	19:18:55	350 sec	11.11	209.9
2	25-Mar-06	12:34:44	99 sec	11.58	244.3
3	20-Jun-06	18:31:16	54 sec	-	-
4	04-Jan-08	10:53:35	641 sec	13.81	196.0
5	22-Feb-08	21:59:38	797 sec	3.44	282.8
6	23-Feb-08	21:59:37	804 sec	3.63	180.2
7	24-Feb-08	21:59:42	776 sec	3.63	230.5
8	27-Feb-08	21:59:38	300 sec	-	-
9	14-May-08	13:11:03	607 sec	1.86	312.3
10		13:59:41	1068 sec	1.40	289.1
11		14:59:38	794 sec	1.46	339.6
12		15:59:38	789 sec	1.23	291.8
13		23:59:38	790 sec	1.29	258.8
14	21-May-08	13:59:38	779 sec	7.46	248.7
15		14:59:37	793 sec	9.18	267.9
16		15:59:37	793 sec	9.30	262.2
17		23:59:38	800 sec	6.43	297.5
18	22-May-08	13:59:37	799 sec	5.90	182.8
19		14:59:40	779 sec	6.46	170.2
20		15:59:38	782 sec	6.09	170.7
21		23:59:37	805 sec	7.25	261.3

Response Measurements

The 17 data sets analyzed in this study to build baseline modal properties of the NCB cover various characteristics of structural responses in time and frequency domains. For instance,

the peak accelerations of the data sets vary from 3.08 to 26.56 cm/sec^2 in vertical direction (at Ch 32 and Ch33) and from 0.41 to 4.16 cm/sec^2 in transverse direction (at Ch 35) at mid-span, and from 0.39 to 2.99 cm/sec^2 (at Ch15) in longitudinal direction.

Figures 2 and 3 present typical time histories of accelerations having different features. In comparison with the time histories from data set #4 in Figure 2, those from data set #21 in Figure 3 exhibit a nonstationary property of having time-varying mean square values. The appearance of such large peaks in a predominantly small amplitude signal is responsible for the nonstationarity of the signal and is linked to the high frequency contents in the signals. Figures 4(a) and (b), which displays normalized power spectral density estimates of the time histories in Figures 2 and 3, respectively, indicate that structural responses of data set #4 are characterized mostly by low frequencies of less than 1 Hz while those of data set #21 are under significant influence of the frequencies between 0 and 1Hz as well as between 3 and 5Hz.

In this study, since the analysis is focused on the identification of primary structural modes, usually in the frequency range of less than 1Hz, the measurements were filtered by using a Butterworth low-pass filter of the ninth order with a cutoff frequency of 1.1Hz.

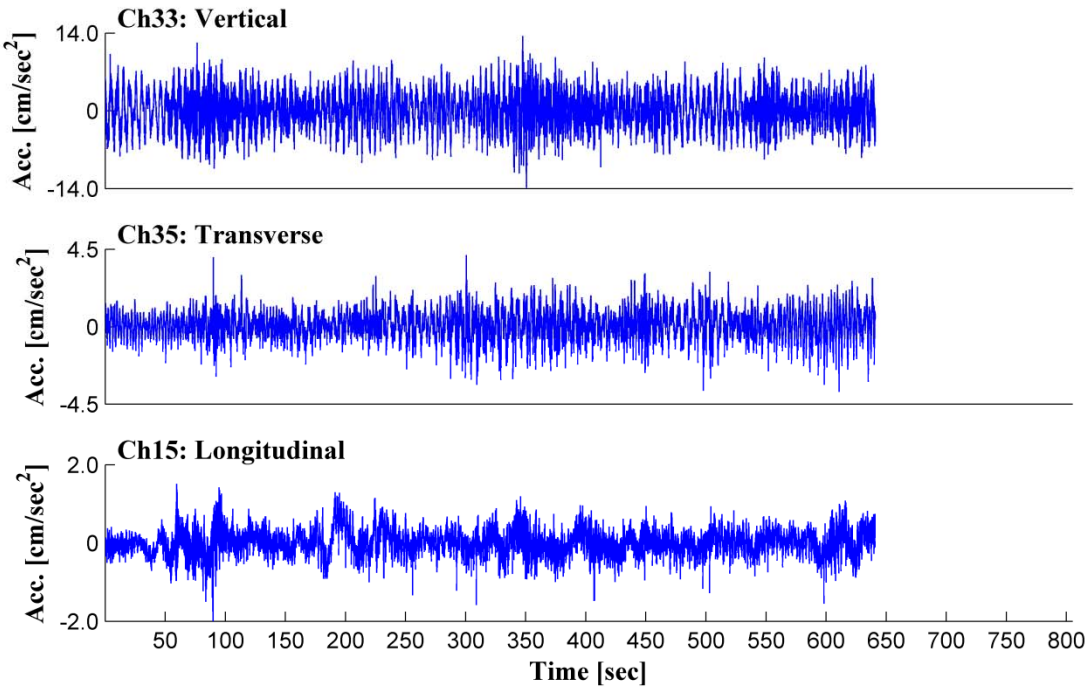

Figure 2. The time histories of acclerations in data set #4

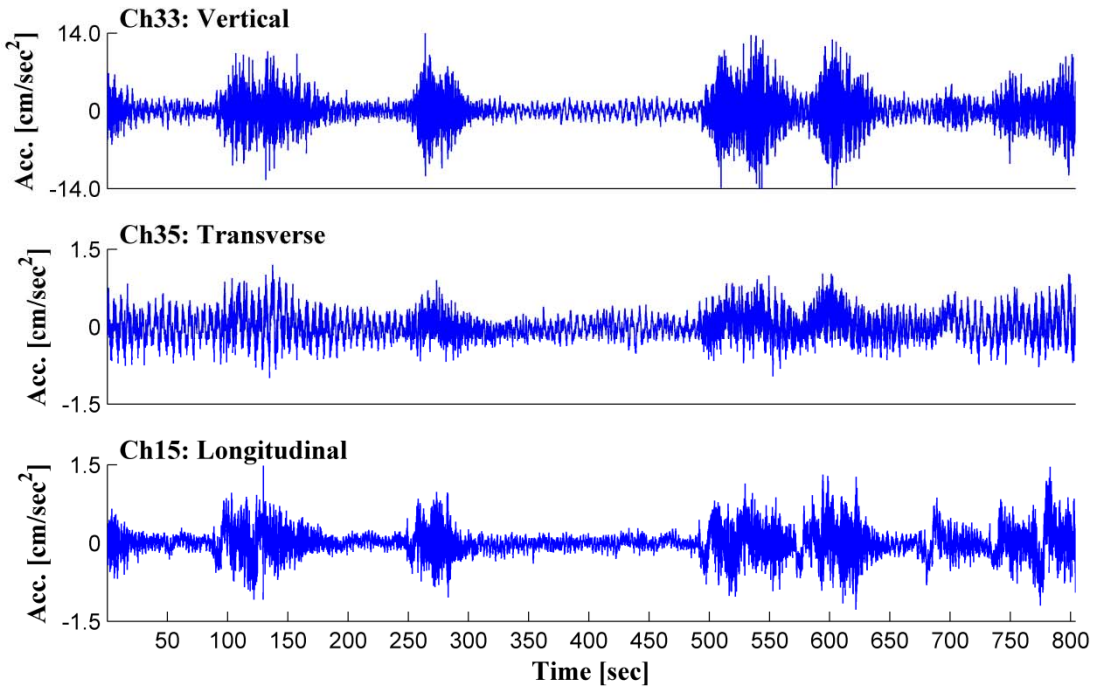

Figure 3. The time histories of acclerations in data set #21

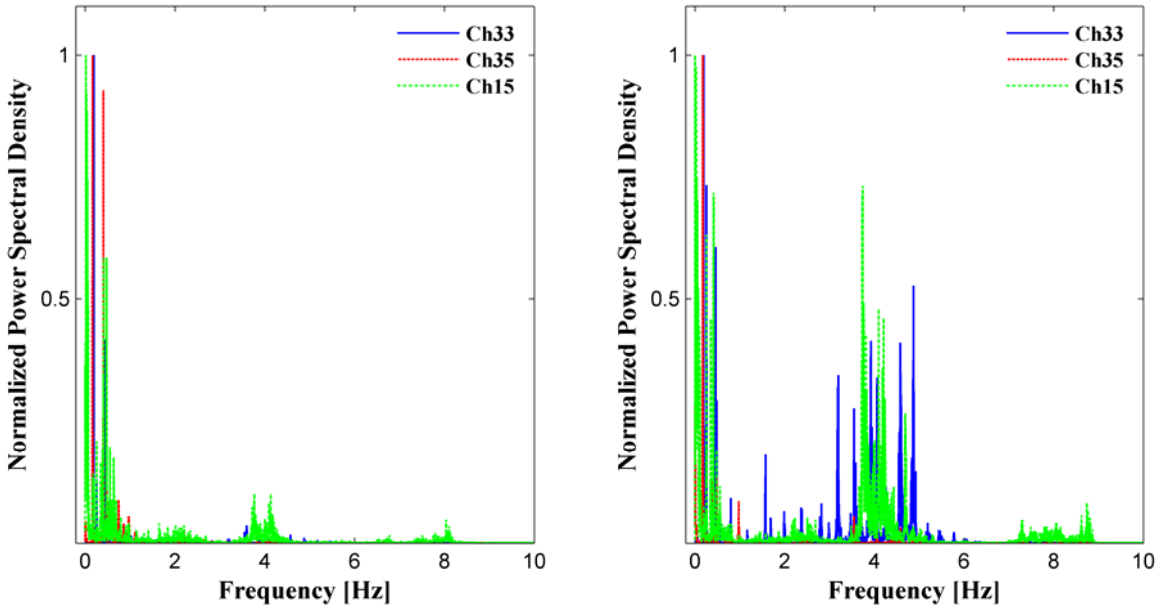

(a) data set #4 **(b)** data set #21

Figure 4. Normalized power spectral density

In addition, the statistical properties of the filtered output observations were examined since the SSI technique presumes that a structural process be Gaussian process. Figure 5 presents the peak acceleration, kurtosis, and skewness of Chs 33 (vertical), 35(transverse), and 15 (longitudinal). Based on the fact that for the Gaussian distribution, the kurtosis and skewness are supposed to be 3 and 0, respectively, vertical and transverse measurements generally show characteristics similar to those of a Gaussian distribution while longitudinal measurements appear to have large values of kurtosis. Since Ch 15 is placed on the deck, at a location where the deck is connected to the tower with the rocker links, it might induce noticeable outliers so to result in a large measure of kurtosis.

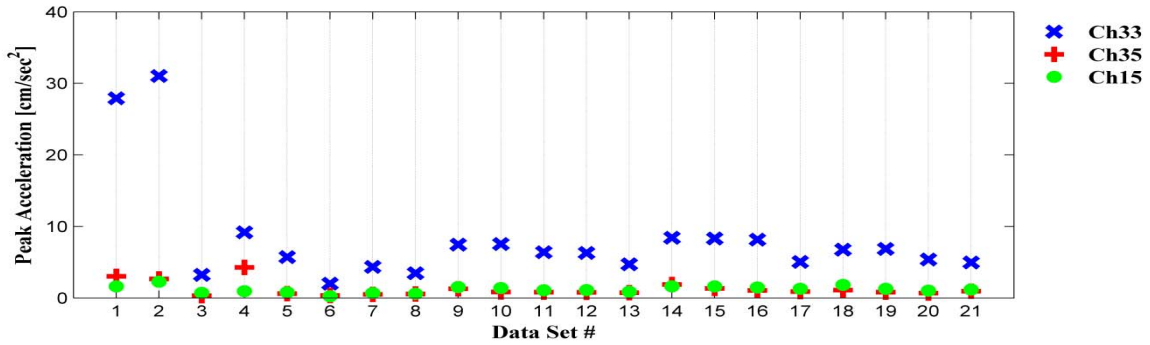

(a) Peak Acceleration

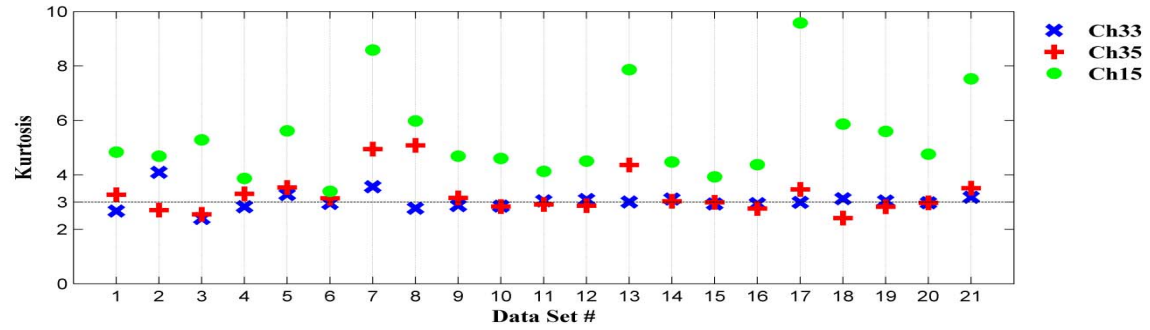

(b) Kurtosis

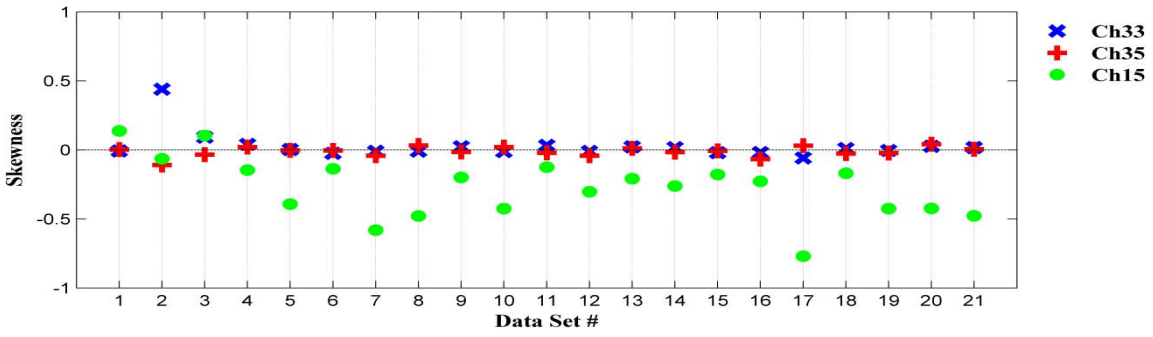

(c) Skewness

Figure5. Statistical properties of response measurements

Data-Driven Stochastic Subspace Identification

Mathematical Models

Stochastic subspace identification technique was established based on stochastic state-space and its innovation (Kalman filter) models. An n^{th}-order linear time-invariant stochastic system with m output observations can be represented in the form of a stochastic discrete-time state-space model such as

$$\begin{aligned} x(k+1) &= A\,x(k) + w(k) \\ y(k) &= C\,x(k) + v(k) \end{aligned} \tag{1}$$

where $x(k) \in \Re^{n\times 1}$ and $y(k) \in \Re^{m\times 1}$ are state and output vectors at time k, respectively, and $A \in \Re^{n\times n}$ and $C \in \Re^{m\times n}$ are, respectively, system and observation matrices. The vectors $w(k) \in \Re^{n\times 1}$ and $v(k) \in \Re^{m\times 1}$ represent process and measurement noises, respectively, and are assumed to be zero-mean white Gaussian processes with covariance matrices: $\mathbf{E}[w(k)w^T(j)]=Q\delta(k-j)$, $\mathbf{E}[v(k)v^T(j)]=R\delta(k-j)$, and $\mathbf{E}[w(k)v^T(j)]=S\delta(k-j)$, where $\delta(k-j)$ is an identity matrix when $k=j$ and zero when $k\neq j$.

When the state vector needs to be estimated with only output observations in the absence of input information, an optimal estimate of $x(k)$, denoted by $\hat{x}(k)$, might be the one that has the minimum variance with respect to $x(k)$. Such an optimal state estimate, can be derived by applying a Kalman filter to Eq. (1) in the following forms [6]

$$\begin{aligned} \hat{x}(k+1) &= A\hat{x}(k) + K\,e(k) \\ e(k) &= y(k) - C\,\hat{x}(k) \end{aligned} \tag{2}$$

where $K \in \Re^{n\times m}$ indicates a Kalman filter gain matrix and $e(k) \in \Re^{m\times 1}$ is the output residual vector having a property of being a zero-mean, white noise process. From Eq. (2), it can be readily observed that the Kalman state vector at the current time k is expressed by a linear combination of the past output vector sequence so to be defined on the past output space.

Data-driven Stochastic Subspace Identification

Considering that the Kalman state vector $\hat{x}(k)$ demands past i output observations (i.e. $y(j), j=k-1, k-2, \ldots, k-i$) for its estimation, past and future output block matrices can be formed [7], respectively, as

$$Y_p = \begin{bmatrix} y(0) & y(1) & \cdots & y(j-1) \\ y(1) & y(2) & \cdots & y(j) \\ \vdots & \vdots & \cdots & \vdots \\ y(i-1) & y(i) & \cdots & y(i+j-2) \end{bmatrix} \text{ and } Y_f = \begin{bmatrix} y(i) & y(i+1) & \cdots & y(i+j-1) \\ y(i+1) & y(i+2) & \cdots & y(i+j) \\ \vdots & \vdots & \cdots & \vdots \\ y(2i-1) & y(2i) & \cdots & y(2i+j-2) \end{bmatrix} \tag{3}$$

where the index *j* is assumed to be infinite because, in the derivation of the SSI method, certain statistical properties (e.g. output covariance) need to be computed directly from Y_p and Y_f under the assumption that the sequence of output observations in each row of both Y_p and Y_f be an ergodic process. Then, the orthogonal projection of the row space of Y_f onto the row space of Y_p can be formulated in terms of the so-called observability matrix (Γ_i) and the Kalman state vector sequence ($\hat{X}_i$) such as

$$O_i = Y_f / Y_p = \begin{bmatrix} C \\ CA \\ CA^2 \\ \vdots \\ CA^{i-1} \end{bmatrix} \begin{bmatrix} \hat{x}(i) & \hat{x}(i+1) & \cdots & \hat{x}(i+j-1) \end{bmatrix} = \Gamma_i \hat{X}_i \tag{4}$$

Eq. (4) implies that the rank of O_i is equal to the dimension of the state vector, the column space of O_i equal to the column space of Γ_i, and the row space of O_i equal to the row space of $\hat{X}_i$. Hence, the observability matrix and the Kalman state vector sequence can be identified by properly decomposing the projection matrix O_i.

Once the observability matrix Γ_i is obtained through the decomposition process of O_i, the system matrix *A* and the observation matrix *C* can be easily extracted from Γ_i for the modal parameter identification. In addition, when the Kalman filter gain matrix *K* needs to be identified in order to have an innovation model of Eq.(2) completed, the matrices *A* and *C* can be obtained in a least-square sense from the following

$$\begin{bmatrix} \hat{x}(i+1) & \hat{x}(i+2) & \hat{x}(i+3) & \cdots \\ y(i) & y(i+1) & y(i+3) & \cdots \end{bmatrix} = \begin{bmatrix} A \\ C \end{bmatrix} \begin{bmatrix} \hat{x}(i) & \hat{x}(i+1) & \hat{x}(i+3) & \cdots \end{bmatrix} + \begin{bmatrix} w' \\ v' \end{bmatrix} \tag{5}$$

where w' and v' are the Kalman filter residuals so to be able to estimate the Kalman filter gain from the covariances of w' and v'. By using the identified matrices *A*, *C*, and *K*, output observations can be reconstructed from the reformulated equation of Eq.(2) as

$$\begin{aligned} \hat{x}(k+1) &= (A - KC)\hat{x}(k) + K\, y(k) \\ \hat{y}(k) &= C\, \hat{x}(k) \end{aligned} \tag{6}$$

where $\hat{y}(k)$ represents reconstructed output sequence from the identified model.

Subsequently, from the state and observation matrices, modal parameters can be obtained by considering the continuous time equivalent state matrix. When output observations are not contaminated by noise, the dimension of the state matrix can be clearly indicated by singular values of O_i in Eq. (4) and so the modal parameters for the system's modes can be estimated just from a realized model. However, when output measurements are disturbed by noise, the projection matrix O_i has full rank and this makes it difficult to assign a certain order to an identified system model only based on the singular values distribution. Even though it is true

that having a higher order identified model helps in minimizing the error between the measured data and the reconstructed responses from the identified model, this error reduction could be due to noise modes that are now included to improve the fitting between the data sets. For this reason, in the application of the SSI technique using real measurements with noise, the extraction of modal parameters corresponding to structural modes is generally complemented by a Stabilization Diagram (SD). Such a diagram, which represents the identified frequencies as a function of the model's order, highlights modes whose properties do not change significantly when varying the dimension of the state vector; such modes are considered as structural modes. In order to form the SD, an observability matrix is repeatedly formulated from Eq. (4) varying the dimension of the state, which provides different pairs of state and output matrices of corresponding orders. The properties of poles in a model of a certain order are compared with those of a two order larger model and stable and unstable modes are determined on the basis of the identified frequencies, damping ratios and mode shapes.

Implementation of the SSI Technique

The SSI technique complemented by the SD, for modal parameter estimation, involves three practical issues that need to be addresses in its implementation: 1) the order of realized state-space models necessary for a certain number of stable modes to appear in the SD could be extremely high; 2) even when a mode is considered stable between certain orders of realized models, estimates of the mode's properties could vary depending on a selection of the model from which those are extracted; and 3) modal parameter estimates, especially damping ratios, are very sensitive to a choice of the number of block rows i in Eq. (3). In this section, we will discuss these issues and then propose an efficient way of implementing the SSI technique to accurately identify modal parameters from ambient vibration measurements.

The problem related to the dimension of the state required to detect stable modes, can be easily controlled, to some extent, if preliminary information about the range of interest for natural frequencies of the structure under consideration is given. In the case of suspension bridges, it is known that vibrational modes contributing to their global response to ambient excitation are mainly confined in the frequency range from about 0 to 1 Hz and so higher frequency contents in measured signals can be considered as trivial information for the characterization of such bridges' fundamental dynamical properties. Therefore, filtering out higher frequency contents and downsampling time histories (to reduce the Nyquist frequency) lead to a reduction of the order of a realized model to represent signal properties. In addition, applying a proper weighting matrix to the projection matrix in Eq. (3) also can help lowering the necessary dimension of the state vector. In fact, the SSI technique considers three different algorithms (the principal component, canonical variate, and unweighted principal component algorithms) which differ from the set of weighting matrices multiplied by the projection matrix. From a comparative study of the three algorithms in the analysis of two suspension bridges (Vincent Thomas Bridge and the New Carquinez Bridge), it was revealed that the principal component algorithm showed the best performance determining the smallest dimension model capable of properly representing the structure's properties [8].

After distinguishing structural modes from noise modes using the SD, one needs to extract modal parameters of structural modes (i.e. stable modes) from realized models: such

parameters can be computed either at once from one specific model which includes all the stable modes, or from different models for each individual mode. However, it is not always easy to find one specific model with all the stable modes. Indeed, modal parameter estimates, especially damping ratios, are significantly affected by the selection of a model's order.

Figure 6(a) presents a stabilization diagram (with i=100 in Eq. (3)) using the six time histories of vertical accelerations from data set #4 as well as the Power Spectral Density (PSD) plots of the measurements. Such a diagram was built by comparing frequencies, damping ratios,

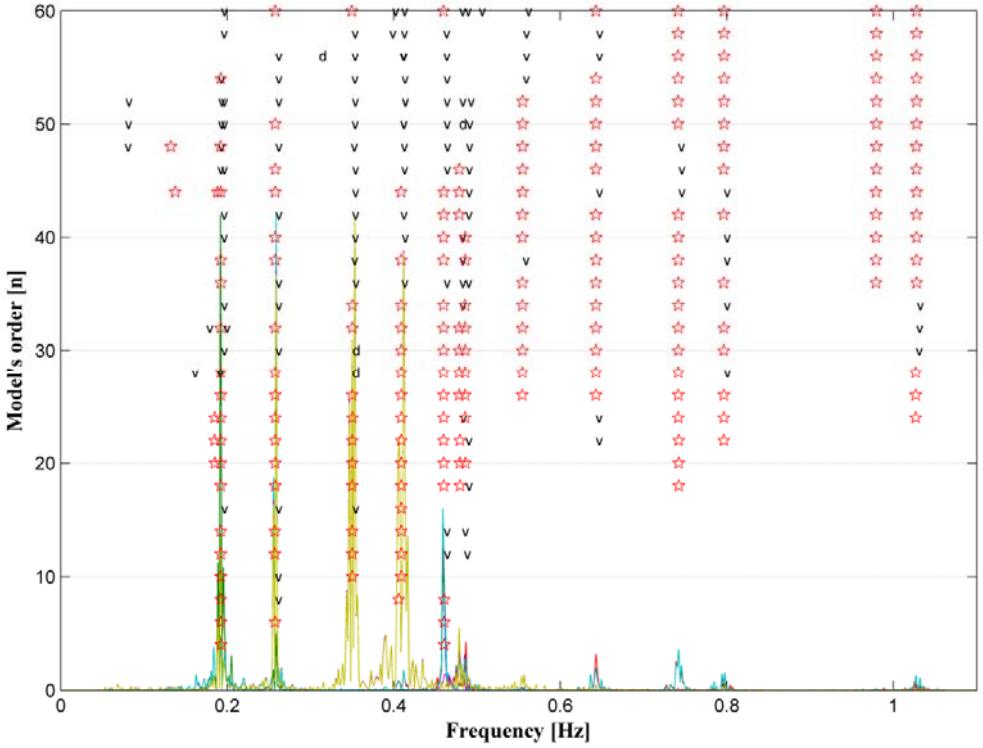

(a) Stabilization diagram

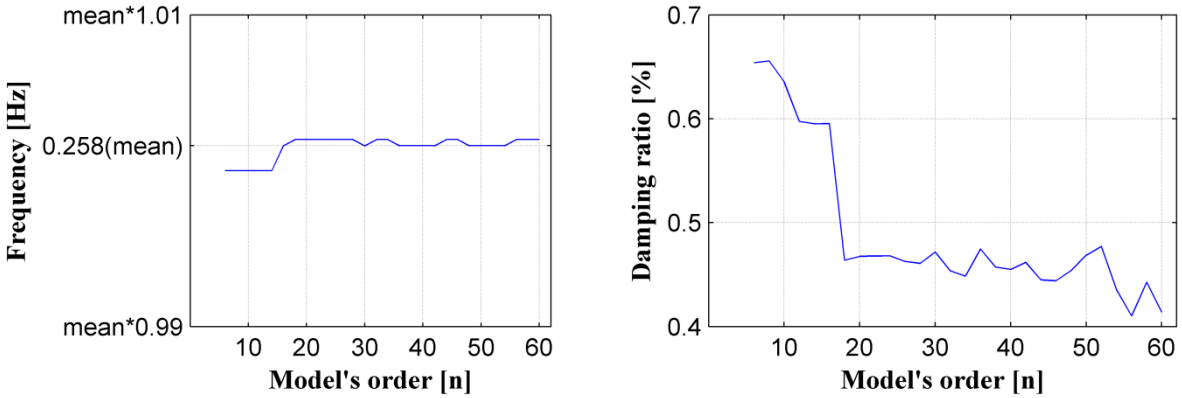

(b) Variations in frequency and damping ratio estimates along model's order

Figure 6. Stabilization diagram and variation in modal parameter estimates

and modes shapes, for each model order, with the corresponding values of a two-order higher model: the frequencies are first compared and modes that have differences of 1% or less in the identified frequencies are retained. Then, the corresponding damping factors and mode shape vectors are compared with stability criteria of 3% difference for the damping and 1% for the mode shape (i.e. MAC>0.99), respectively. In Figure 6(a), a mode that satisfies all the criteria is represented with a 'star', a mode that only satisfies the frequency and mode shape criteria with a 'v', and a mode that only satisfies the frequency and damping ratio criteria with a 'd'. Even though the SD in Figure 6(a) clearly displays modes that are consistent with the frequency peaks of the PSD plots, there is no specific model that includes all the stable modes appearing in Figure 6(a). Moreover, even when modal parameters of stable modes are estimated from different models, a proper selection of a specific model should be made for each mode since the selected model's order can results in large variations of the identified parameters, especially the damping. To explain this, let's consider Figure 6(a) that shows that the mode with the corresponding frequency of about 0.258 Hz is a structural mode. When modal parameters are calculated for such a mode, any model of order ranging between 6 and 56 will provide consistent values of frequency as well as mode shape vector, but not of the damping ratio. Figure 6(b) shows a significant variation in the identified damping ratios ranging from 0.41% to 0.66% as the order of the model decreases. Because damping ratio estimates are more affected by the model's order than the frequency and mode shape, a less restrictive stability criterion is generally assigned to the damping ratio. In this way, the SD is capable of detecting stable modes that satisfy all the criteria; however, because of the loose criterion on the damping, there is an increased possibility of identifying less accurate damping ratios.

For the selection of the order of a realized model for the estimation of the modal parameters, realized system models of different orders were divided into groups, for each mode, in each of which all the modal parameters, including the damping ratio, were consistently stabilized. Among the group covering the largest range of models' orders, the model with the largest dimension of the state vector was selected for the parameter estimation.

With regard to the selection of the number of block rows i, Pridham and Wilson [9] showed that significant variations occurred in the damping ratio estimates for different pairs of i and j in Eq. (3) in the ambient vibration analysis of the Vincent Thomas suspension bridge and also remarked that no definite rule to find an optimal pair of them could be derived from the analysis. For the optimal estimation of damping ratios, the same authors [10] proposed a method that consists in optimizing realized state-space models from the SSI technique through the expectation maximization algorithm. In order to select the best initial models, they found ten models that contain the maximum number of stable modes by taking into account possible combinations of i, j, and n (the system's order).

In this study, rather than obtaining clearly stable modes on the SD by changing the value of i, a relatively simple way of selecting i is proposed based on the error between measured data and reconstructed one from the identified structural modes. Note that, in the theoretical implementation of the SSI technique, the number of block columns j is assumed to be infinite. However, data sets analyzed in this study have record lengths of about 10 min., which cannot be considered long in the ambient vibration analysis, and, consequently, j is automatically determined by the value of i ($j=nd-2\times i+1$ where nd is the number of data points); hence, only an

effect of change in *i* was examined in this study.

The error between measured data and reconstructed one from the identified structural modes can be calculated in the following way. Eq. (6) can be restated in modal coordinates such as

$$\hat{y}(k) = C(\Psi\ \Psi^{-1})\hat{x}(k) = C_m\hat{x}_m(k) \tag{7}$$

where Ψ is the eigenvector matrix of the state matrix A (A= $\Psi\ \Lambda\Psi^{-1}$) and C_m and $\hat{x}_m(k)$ denote $C\Psi$ and $\Psi^{-1}\hat{x}(k)$, respectively. This equation allows us to decompose the reconstructed signal from an identified triple of A, C, and K into each mode's contribution: a contribution of the q^{th} mode to the output observations can be computed as

$$\hat{y}(k)_q = C_m(:,q)\hat{x}_m(k)_q \tag{8}$$

where $\hat{x}_m(k)_q$ represents the q^{th} element of the transformed state vector $\hat{x}_m(k)$ while $C_m(:,q)$ indicates the q^{th} column of the matrix C_m. $\hat{y}(k)_q$ represents the contribution to the total response by the q^{th} mode. From this formulation, the contribution from each specific mode to the overall response can be obtained from the model selected among the models in which this mode is stable. The contributions from different modes can be easily obtained from models of different order, depending on the stability of each mode. Then, the sum of the contribution signals extracted from different models yields the reconstruction of the measurements which is attributed to only structural modes and so the measurement error $\boldsymbol{\varepsilon}(k)$ can be calculated as

$$\boldsymbol{\varepsilon}(k) = y(k) - 2\times\sum_{q=1}^{ns}\hat{y}(k)_q \tag{9}$$

where *ns* denotes the number of stable modes and the number 2 is associated to the fact that modes come in complex conjugate pairs. Based on this error estimate, the optimal value of *i* and, consequently, modal parameter estimates that produce the smallest error can be obtained. Furthermore, a relatively large amount of error could also indicate that some of structural modes that are contained in the measurements fail to be identified in the analysis.

To show this process, consider the analysis which used the same measurements (six vertical accelerations) from data set #4 as those for the SD in Figure 6. In order to examine the effect of a change in *i* on the estimated errors, the value of *i* varied from 20 to 200. The errors obtained at Channels 33, 28, and 6 are presented in Figure 7 in terms of the relative Root Mean Square (RMS) values as a function of *i*. Such a figure implies that values of *i* smaller than 50 cannot be used for a successful implementation of the SSI technique. It also points out that having a larger value of *i* does not guarantee a better result. In fact, the errors between 140 and 200 of *i* are shown to be larger than those between 70 and 130 in Figure 7. In the case of this analysis for data set #4, the optimal value of *i* was selected to be 80 which produced the smallest error on the average of the relative RMS errors at the six channels. Figure 8 exhibits one of the

reconstructed signals with i=80.The reconstructed signal shows a good match with the measured one with the error of 11.97% (0.29 cm/sec^2). It might be worth noting that the optimal is for the analyses of the other data sets also turned out to be between 70 and 130.

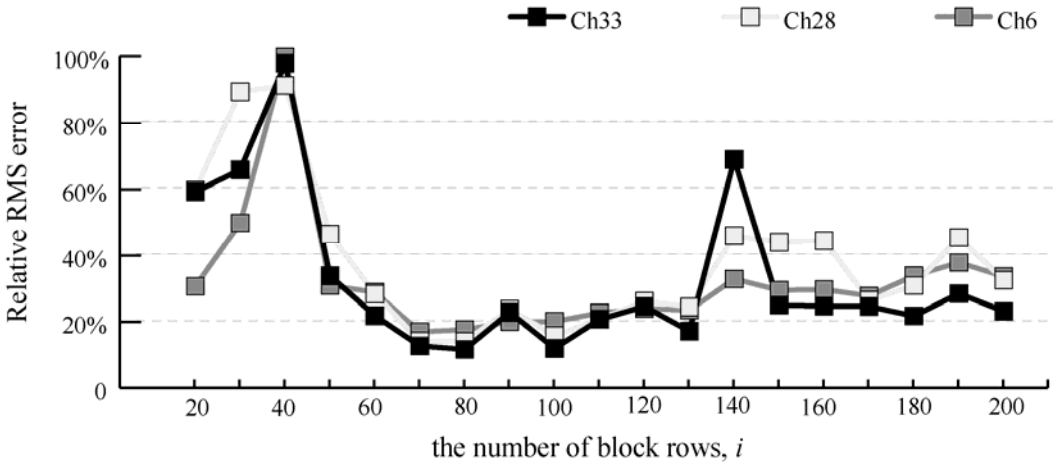

Figure 7. The effect of a change in the number of block rows, i, on relative RMS errors

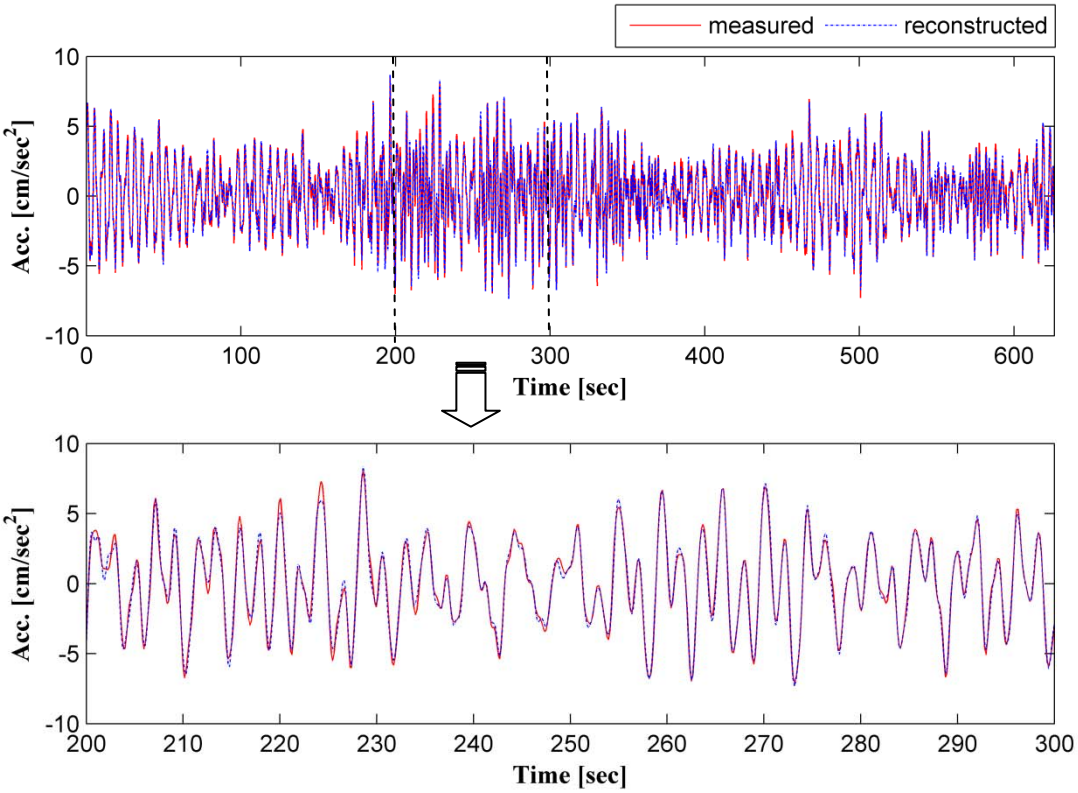

Figure 8. Measured and reconstructed accelerations (at Ch 33) with i=80

Identified Modal Parameters

In this study, structural modes of the Carquinez suspension bridge were classified into four groups: vertical, torsional , transverse, and torsion/transverse (hybrid) modes. Modal properties for vertical and torsional modes were estimated from the analysis using the six time histories of vertical accelerations while those for transverse modes were computed from the analysis using the three time histories of transverse accelerations. For modal parameter estimates of torsion/transverse modes, on the other hand, the six vertical and three transverse acceleration measurements were considered together. Although vertical, torsional, and transverse modes could also be identified when all the measurements in different directions were considered at the same time, it was difficult to obtain, from all the data sets, results as accurate as those obtained when measurements in each direction were separately analyzed. Hence, vertical, torsional, and transverse modes were analyzed using acceleration time histories in the corresponding directions while hybrid modes were identified using all the measurement together making allowances for uncertainty.

In order to classify the identified modes into such groups, it is a priority to characterize such modes' shapes. The identified mode shape vectors are complex and so, at each sensor location, they are characterized by an amplitude and by a phase, which is different from location to location. Hence, because of the phase variation, it is very difficult to plot schematic representation of each mode shape. In addition, since the mode shape vectors are extended to the entire structure by connecting the identified value at the sensors locations by straight lines, the use of the small number of sensors located only on half of the deck made it hard to visualize whether a particular mode is symmetric or anti-symmetric; hence, previous experimental [11] as well as numerical [12] studies on the NCB were cited to help with such a distinction.

With regard to the characterization of hybrid modes, data set #4 was first analyzed, as a representative data set using all the ten measurements in the three directions (vertical, transverse, and longitudinal). Since, among those available, data set #4 was recorded when the NCB experienced the strongest wind, a relatively large number of structural modes including hybrid modes was well excited to be clearly identified. Based on these mode shapes identified from data set #4, it was possible to distinguish torsional and transverse modes from hybrid torsional/transverse modes when measurements in the vertical and transverse directions were separately used in the analysis. Furthermore, considering the measurement in the longitudinal direction also allowed us to represent a hybrid longitudinal/vertical mode. In fact, there was a specific mode which displayed a longitudinal displacement while exhibiting a symmetric shape in the vertical direction. Such a mode was classified neither symmetric nor anti-symmetric in the study by Conte *et al*. [11] since, in the identification, the authors utilized only the time histories of the vertical response on the main deck.

Tables 2 and 3 present the natural frequencies and damping ratios, identified from the 17 data sets, for vertical modes and for torsional, transverse, and torsion/transverse modes, respectively, with those presented in the studies by Conte *et al*. [11] and Scanlan and Jones [12]. The identified mode shapes that correspond to those in Tables 2 and 3 are displayed Figures 9 and 10, respectively. Note that not all the modes were consistently identified from all the data sets because the only modes that could be identified were those that were contained in the

measurements and not all of them were equally excited. The identified frequencies in this study show a good agreement with those from the other studies, except one corresponding to the first anti-symmetric mode (V1 in Table 2). While the mode occurred with the frequency of 0.15 Hz in the numerical study [12], higher frequencies were identified for such mode in the experimental studies including the current study: 0.201Hz in the study by Conte *et al*. [11] and between 0.179 and 0.197 Hz in this study. With regard to damping ratios, the damping ratios identified in this study appear to be, in general, larger than those in the study by Conte *et al*. [11]. One of the reasons for such a discrepancy might be in the difference in the analyzed data: 20 min long ambient vibration data was used in Conte *et al*. [11], which is almost twice as long as the ones used in this study.

Variability of Modal Parameters

Modal parameters represent a structure's dynamic properties and could be used to detect structural damage. In fact, the appearance of damage could be reflected by a change in such parameters. However, since the estimates of modal parameters can also vary because of different environmental and operational conditions (such as temperature, wind, humidity, and traffic flow), it is important, for a given structure, to understand the variability of such parameters with the environmental factors so to distinguish their effects from those induced by structural damage.

Recently, various studies have been performed about effects of different environmental and operational conditions on the variability of modal parameters, especially fundamental natural frequencies of long-span bridges such as suspension and cable stayed bridges. With regard to temperature effect, Sun *et al.* [13],with continuously monitored data for 8 months from Donghai cable-stayed bridge in China, and Kang *et al.* [14], with continuously monitored data for 5 years from Seohae cable-stayed bridge in Korea, showed that fundamental frequencies of such long span bridges decreased when the temperature increased. Using 288 data sets for weekdays and 123 for weekends recorded from Vincent Thomas suspension bridge in the United States, Yun *et al*. [15] presented differences in the identified frequencies and damping ratios between weekdays and weekends. Also, Abe *et al*. [16] pointed out, from the analysis using continuously measured data over 100 hours from Hakucho suspension bridge in Japan, that the identified natural frequencies were reduced as wind velocity became higher while the identified damping ratios started to increase when wind velocity reached at a certain level.

In this study, from the investigation of effects of wind speed on the identified frequencies and damping ratios, it was observed that when wind speed increased, the identified natural frequencies for certain modes decreased while the identified damping ratios increased, as presented in Abe *et al*. [16]. Also, in comparing the results from the data sets recorded at different times on the same days (data sets #9 to 13, data sets #14 to 17, and data sets #18 to 21), variations in the identified frequencies and damping ratios during a day were found. Nevertheless, because of the limited number of the data sets used in this study, it was difficult to clearly define such effects on the identified modal parameters. Additional data sets continuously or periodically recorded would help to investigate the variability of such modal parameters, reducing uncertainties in the estimates.

Table 2. Identified natural frequencies and damping ratios for vertical (V) modes

Mode	Frequencies (Hz)			Damping ratios [%]		Description
	This study	[1]*	[2]†	This study	[1]*	
V1	0.179 - 0.197	0.201	0.15	2.25 - 6.97	1.36	Anti-symmetric
V2	0.192 - 0.196	0.193	0.19	0.26 - 1.49	0.21	Symmetric
V3	0.257 - 0.259	0.258	0.25	0.04 - 0.96	0.23	Symmetric
V4	0.347 - 0.352	0.350	0.36	0.07 - 0.57	0.20	Anti-symmetric
V5	0.402 - 0.413	0.414	0.39	0.47 - 2.17	0.13	Anti-symmetric: north-span
V6	0.476 - 0.485	0.483	0.48	0.30 - 0.49	0.21	Symmetric
V7	0.555 - 0.563	0.561	0.54	0.35 - 1.05	0.15	Symmetric/longitudinal
V8	0.638 - 0.648	0.645	0.68	0.15 - 0.55	0.11	Anti-symmetric
V9	0.789 - 0.801	0.799	-	0.13 - 0.53	0.23	Symmetric

*: the study by Conte et al. [11]; and †: the study by Scanlan and Jones [12]

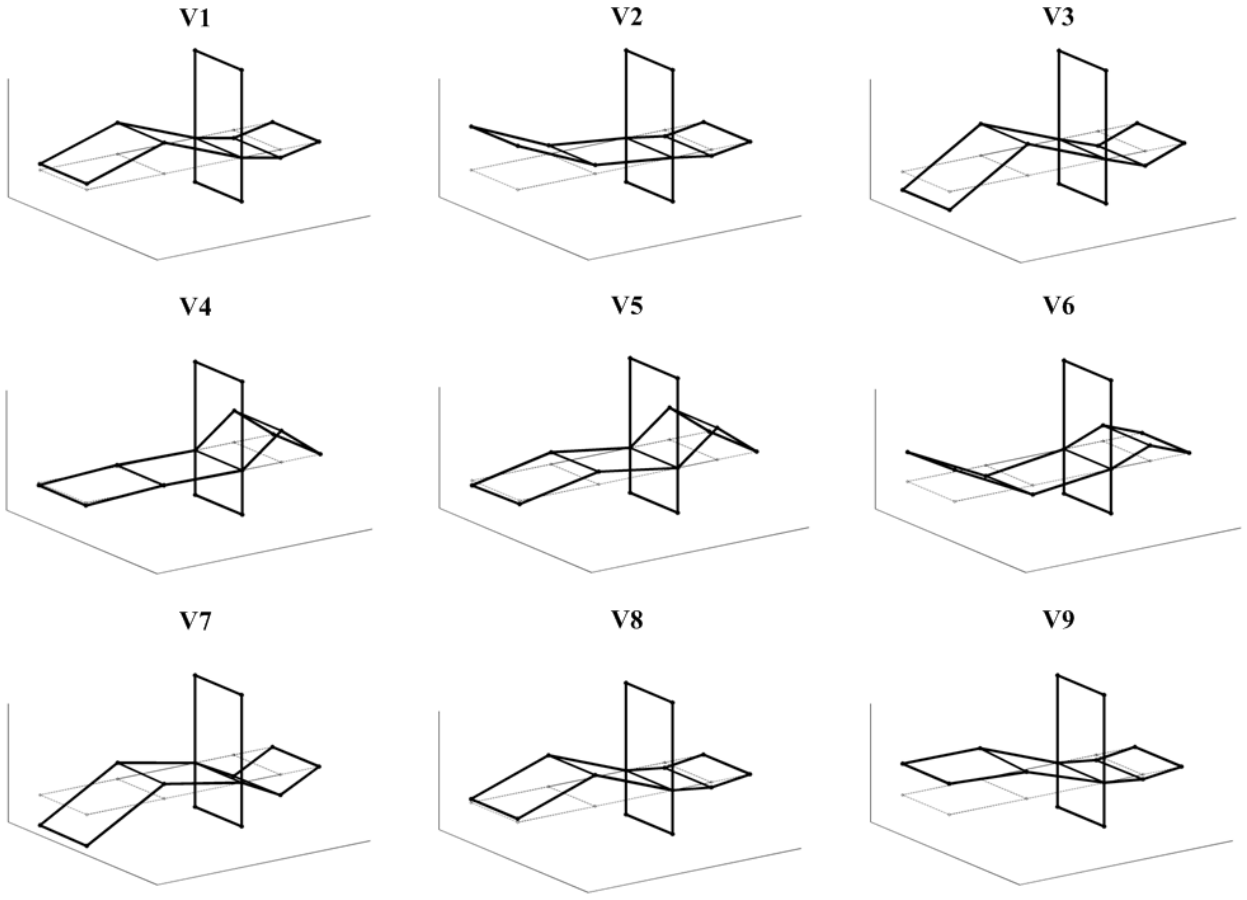

Figure 9. Identified mode shapes for vertical (V) modes

Table 3. Identified natural frequencies and damping ratios for torsional (T), transverse (Tr), and torsion/transverse (TTr) modes

Mode	Frequencies [Hz]			Damping ratios [%]	
	This study	[1]*	[2]†	This study	[1]*
T1	0.458 - 0.469	0.471	0.47	0.05 - 1.18	0.17
T2	0.735 - 0.744	0.741	0.75	0.03 - 0.58	0.34
T3	1.022 - 1.038	-	1.03	0.10 - 0.53	-
Tr1	0.162 - 0.177	-	0.17	0.36 - 1.39	-
Tr2	0.365 - 0.375	-	0.31	0.16 - 1.06	-
Tr3	0.520 - 0.538	-	-	0.23 - 0.58	-
TTr1	0.475 - 0.490	-	-	0.05 - 0.24	-
TTr2	0.500 - 0.510	-	0.58	0.23 - 0.41	-
TTr3	0.940 - 0.978	-	-	0.55 - 0.89	-

*: the study by Conte et al. [11]; and †: the study by Scanlan and Jones [12]

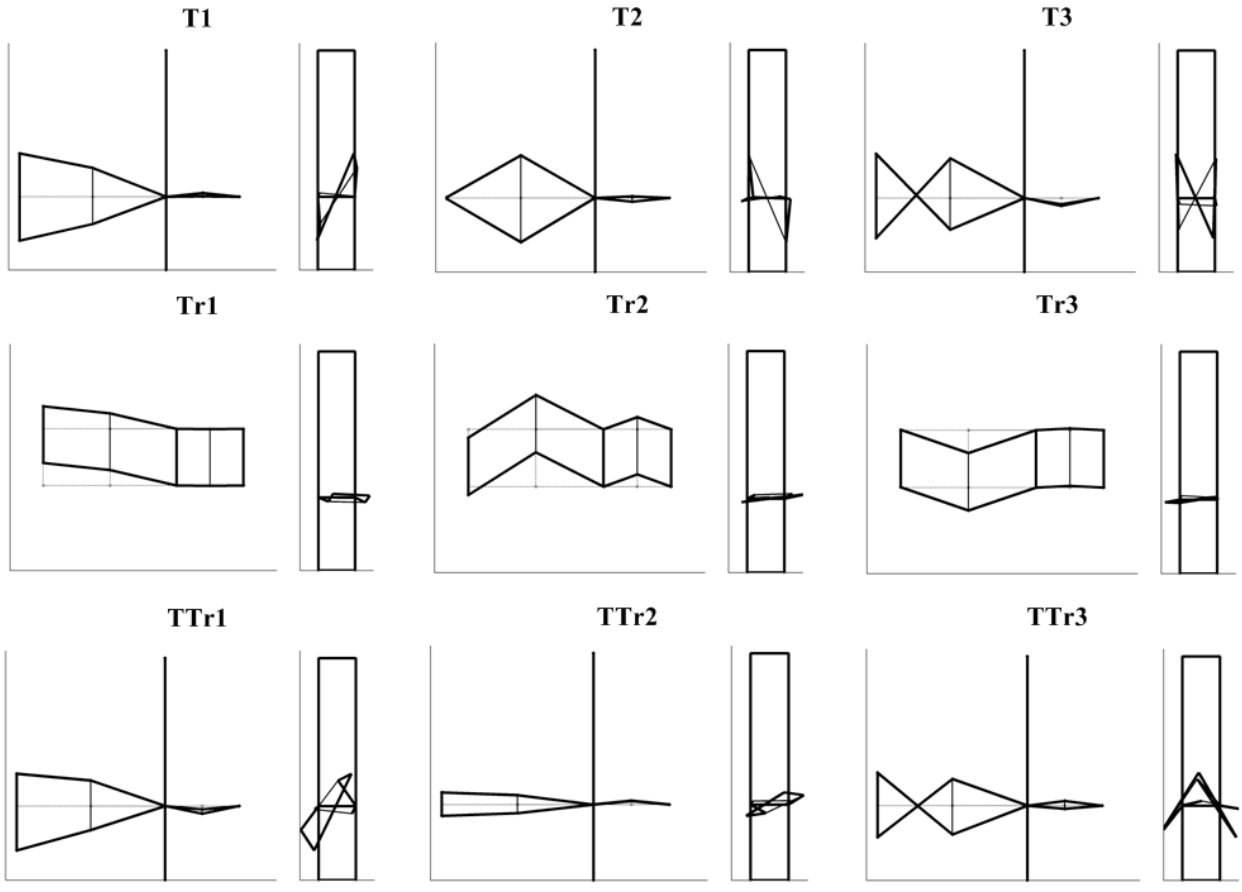

Figure 10. Identified mode shapes for torsional (T), transverse (Tr), and torsion/transverse (TTr) modes

Conclusions

The characterization of dynamic properties of the New Carquinez suspension bridge has been performed by identifying its natural frequencies, damping ratios, and mode shapes, using 17 ambient vibration data sets recorded through the wind-motion monitoring system. By presenting certain bounds of modal parameter estimates for each structural mode identified from the 17 data sets, baseline modal parameters of the bridge were provided for the evaluation of its dynamical behavior in operating condition.

To this end, the data-driven SSI technique was implemented for modal parameters identification, complemented by a stabilization diagram. In the implementation of such technique, three practical issues were first investigated: 1) the dimension of the state needed for a certain number of stable modes to appear in SD; 2) the selection of the order of a realized state-space model to extract stable modes' modal parameters; and 3) the selection of the number of block rows *i* for the projection matrix. After that, the modal parameters for structural modes were identified, for each data set, by examining the estimation error between measured data and reconstructed one from the identified modes.

The identified structural modes of the NCB were represented, in this study, by four groups of modes (vertical, torsional, transverse, and hybrid torsion/transverse modes). Using the acceleration measurements in three orthogonal directions together in the analysis made it possible to characterize the hybrid modes' shapes as well. The frequencies and damping ratios identified in this study showed a good agreement with those presented by the other studies on this bridge. Even though it was observed that the identified frequencies and damping ratios were affected, in a certain way, by the change of wind speed, it was difficult to clearly define such effects because of the limited number of data sets used in this study. For a more in-depth investigation of the variability of damping ratios as well as natural frequencies, additional data sets are needed.

Acknowledgements

The authors would like to acknowledge the support of the California Strong Motion Instrumentation Program (Award number: 1006-903, Project Manager: Dr. Moh Huang) in providing data and resources for the completion of this study.

References

[1] Peeters, B. and De Roeck, G. (2001). "Stochastic system identification for operational modal analysis: a review." *Journal of Dynamic Systems, Measurement, and Control*, **123**: 659-667.

[2] Peeters, B. and Ventura, C.E. (2003). "Comparative study of modal analysis techniques for bridge dynamic characteristics." *Mechanical Systems and Signal Processing*, **17**(5): 965-988.

[3] Zhang, L. Wang, T. and Tamura, Y. (2005). "Frequency-spatial domain decomposition (FSDD) technique for operational modal analysis." *Proceedings of the 1st International Operational Modal Analysis Conference*, Copenhagen, Denmark.

[4] Yu, D.J. & Ren, W.X. (2005). "EMD-based stochastic subspace identification of structures from operational vibration measurements." *Engineering Structures*, **27**: 1741-1751.

[5] Brincker, R., Frandsen, J.B., and Andersen, P. (2000). "Ambient response analysis of the Great Belt Bridge." *Proceedings of the 18th International Modal Analysis Conference*, San Antonio, Texas.

[6] Juang, J. (1994). *Applied System Identification*. Upper Saddle River: Prentice Hall PTR.

[7] Van Overschee, P. and De Moor, B. (1996). *Subspace Identification for Linear Systems – Theory, Implementation, Applications*. Boston: Kluwer Academic Publishers.

[8] Hong, A.L. & Betti, R. (2008). "Identification of the dynamic characteristics of long span bridges using ambient vibration measurements." *Proceedings of the 4th International Conference on Bridge Maintenance, Safety and Management*, Seoul, Korea.

[9] Pridham, B.A. & Wilson, J.C. (2003). "An application example illustrating the practical issues of subspace identification." *Proceedings of the 21st International Modal Analysis Conference*, Kissimmee, Florida.

[10] Pridham, B.A. & Wilson, J.C. (2005). "A reassessment of dynamic characteristics of the Quincy Bay Bridge using output-only identification techniques." *Earthquake Engineering and Structural Dynamics*, **34**: 787-805.

[11] Conte, J.P., He, X., Moaveni, B., Masri, S.F., Caffrey, J.P., Wahbeh, M. Tasbihgoo, F., Whang, D.H and Elgamal, A. (2008). "Dynamic Testing of Alfred Zampa Memorial Bridge." *Journal of structural engineering*, **134**(6): 1006-1015.

[12] Scanlan, R.H. and Jones, N.P. (1998). *Wind Response Study Carquinez Strait Suspended Span*, Report for West Wind Laboratory, Inc. and OPAC Consulting Engineers.

[13] Sun, Z., Min, Z.H. and Zhou, Z.F. (2008). "Baseline knowledge discovery from one-year structural monitoring measurements of Donghai Bridge." *Proceedings of the 4th International Conference on Bridge Maintenance, Safety and Management*, Seoul, Korea.

[14] Kang, S.G., Kwon, J.B., Lee, I.K., and Lee, G.H. (2008). "Structural behaviors of Seohae cable-stayed bridge affected by temperature." *Proceedings of the 4th International Conference on Bridge Maintenance, Safety and Management*, Seoul, Korea.

[15] Yun, H.B., Masri, S.F., Nayeri, R.D., Tasbihgoo, F, Kallinikidou, E., Wahbej, M., Wolfe, R.W., and Sheng, L.H. (2008). "Long-term monitoring of the stochastic characteristics of a full-scale suspension bridge." *Proceedings of the 4th International Conference on Bridge Maintenance, Safety and Management*, Seoul, Korea.

[16] Abe, M. Fujino, Y., Yanagihara, M., and Sato, M. (2000). "Monitoring of Hakucho suspension bridge by ambient vibration measurement." *Proceedings of SPIE*, **3995**:237-244.